Proceedings of the 7th International Symposium on Cavitation
CAV2009 – Paper No. 90
August 17-22, 2009, Ann Arbor, Michigan, USA

Generality of Rotating Partial Cavitation in Two-Dimensional Cascades

Byung-Jin AN
Osaka University Graduate School
Suita, Osaka, JAPAN

Takeo KAJISHIMA
Osaka University
Suita, Osaka, JAPAN

Kie OKABAYASHI
Osaka University Graduate School
Suita, Osaka, JAPAN

ABSTRACT

Numerical simulations of 2-dimensional (2D) unsteady cavitating flows were carried out under various conditions of the number of blades, incidence angles and cavitation numbers. When the incidence angle increased or the cavitation number decreased, the steady balanced cavitation transited to unsteady and non-uniform patterns. Typical patterns reported in the previous studies such as rotating, asymmetric and alternating for 3- and 4-blades were successfully reproduced. In this study, cascades of the larger number of blades were dealt with to consider the generality of unsteadiness by reducing the influence of periodicity. The cavitation is basically triggered in the backward next section. However, the period of time for growing causes complexity in the discrimination of propagation. In most cases of rotating partial cavitation, except for 4-blades, the cavity develops in the second passage of backward direction after the decay of largest cavity. In case of many blades, multiple cavities rotate simultaneously and the particular patterns observed in cascades of small even numbers of blades attenuate.

Key Words : Cavitation, Inducer, Numerical Simulation, Turbomachinery, Unsteady Flow, Cascade, Gas-Liquid Two-Phase Flow

INTRODUCTION

A typical example of the high-speed hydro-machineries is the inducer of a liquid fuel rocket engine, which is the target of this research. In case of a rocket engine, since weight and performance have an important effect on payload, it is crucial to perform studies about high speed in order to improve performance and lower the weight. The generation of cavitation in high-speed hydro-machinery sometimes results in serious accidents. During the development stage of the LE-7 rockets in Japan, it was pointed that cavitation is the cause of axial vibration [1]. However, it is actually difficult to perform experimental studies on real working fluid.

Tsujimoto, et al. developed the linear theory to derive the stability condition in cavitating flow through cascade. It is useful for the prediction of the rotating cavitation. And they analyzed behavior of unsteady cavitation by a linear analysis and singular point method [2-4].

Numerical simulations in order to investigate the properties of the flows at the cavitation condition, based on the Navier-Stokes equation, started from 1990's. Cavitation usually involves strong unsteadiness and can have various types like bubbles, sheets, clouds, vortices, etc. Also, in the unsteady phenomena which occur in the cascade, various modes are observed, like rotating cavitation, alternating cavitation, cavitation surge, etc. Therefore, research on numerical simulation technology, which can deal with various modes of unsteady cavitations, continues.

The authors reproduced an unsteady cavitating flow field in a 2D cascade [5-6] and in a 3D inducer [7], using their simulation method. On the other hand, by a barotropic model, Iga, et al. [8] and Fortes-Patella, et al. [9] analyzed unsteady cavitating flows in 2D models. Coutier-Delgosha, et al. [10] conducted 3D simulation for a 3D inducer. Recently, Yamanishi, et al. [11] applied LES to the 3D turbulent flows including a cascade.

An inducer with 3- or 4-blades is necessary in order to raise the pressure in front of main engine. In case of the LE-7A engine of the H-IIA rocket in JAPAN, 3-blades inducer is used, the Vulcain engine of Ariane rocket in Europe and the Space Shuttle Main Engine in USA used an inducer of 4-blades. Therefore, conventional experiments and analyses are based on 3- and 4-blades cascade. However, it is generally difficult to deal with behavior of the non-synchronous cavitation because the influence of the periodicity in a few numbers of blades is strong. Namely, in Fig. 1, when cavitation propagates to the passage next, the flow passage is same 2nd to the opposite direction in case of 3-blades cascade. Also, in case of 4-blades cascade, the propagation of cavitation to the ±2nd passage is a same and a rotating symmetry at the same time. For these

reasons, it is difficult to understand that relationship between the directions which cavitation affects and the passage which appears clearly next.

The objective of this study is to find generality in the rotating cavitation. And larger number of blades is considered to reduce the influence of the periodicity which appears 3- and 4-blades cascade. First, the results of the prime numbers which are 5-, 7- and 11-blades cascades are explained. Then, the 6- and 8-blades cascades are treated to observe how alternating cavitation to be appeared. Finally, generality about the propagation of unsteady cavitation is considered.

2. OUTLINE OF COMPUTATION

2.1 Computational setup

In this study, a flow through 2D cascades of flat blades is considered. The computational domain shown in Fig. 1 is approximated to the tip region in an inducer of a liquid fuel rocket engine. The chord length and the pitch are C and h respectively. The pitch chord ratio h/C is 0.5 and the stagger angle β = 71.4°. The inflow boundary of the computational region is at $4C$ upstream from the leading edge of the blades, the outflow boundary is at $5C$ from the trailing edge.

The blades are numbered as: B.1, B.2, … , B.N. The flow passages between blades are numbered as P.1-2, P.2-3, and the last passage becomes P.N-1 due to periodicity.

An H-type grid in a curvilinear coordinate system is generated. The number of grid points is 160×40 in each passage. The non-slip condition is applied at the blade surface, the non-uniform grid near the blade surface, especially in the vicinity of leading and trailing edges, is generated with high resolution. The H-type grids of the passages next to the boundary are connected to circumferential direction of cascade, and the periodic condition is set at both ends.

The uniform inlet velocity and the incidence angle are fixed in each simulation. The convective outflow boundary condition and the non-slip condition on the solid walls are applied. Specially, the non-reflective boundary condition is used on the pressure equation [12]. At this time, the pressure p_∞ in a far downstream L_∞ will be fixed. The saturated vapor pressure p_v is given from the cavitation number using a reference pressure p_∞. Eq. (1) is the cavitation number:

$$\sigma = \frac{p_\infty - p_v}{\frac{1}{2}\rho_l u_{in}^2} \tag{1}$$

where u_{in} is inlet velocity and ρ_l is the density of liquid.

2.2 Governing equations

Hereafter, all variables are non-dimensionalized by a characteristic length C, velocity u_{in} and the liquid density ρ_l. Also, the flow field is assumed to be isothermal.

The total density becomes $\rho = f_l \rho_l$ when liquid is treated homogeneously, because the vapor is assumed as a cavity of density 0. At this time, f_l is the liquid volume fraction. The liquid is considered as weakly compressible and a low-Mach number assumption is applied to the mass conservation equation, which can be expressed as:

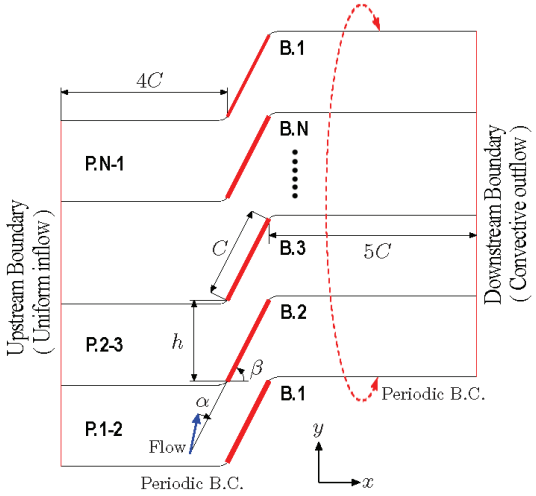

Figure 1: Computational domain and boundary conditions

$$\frac{Df_l}{Dt} + f_l \left\{ M^2 \frac{Dp}{Dt} + \frac{1}{J} \frac{\partial (JU)^j}{\partial \xi^j} \right\} = 0 \tag{2}$$

The momentum equation considering f_l, can be written as follows:

$$\frac{du_i}{dt} + U^j \frac{\partial u_i}{\partial \xi^j} = -\frac{1}{f_l} \frac{\partial \xi^k}{\partial x_i} \frac{\partial p}{\partial \xi^k} + \frac{1}{J} \frac{\partial}{\partial \xi^k} \left\{ \left(\frac{1}{Re} + \nu_T \right) J \frac{\partial \xi^k}{\partial x_j} \left(\frac{\partial u_i}{\partial x_j} + \frac{\partial u_j}{\partial x_i} \right) \right\} \tag{3}$$

Where x_i is the Cartesian coordinate, ξ^j is the curvilinear coordinate and J is the Jacobean of the coordinate transformation. u_i is x_i direction component of the velocity, U^j is the contra-variant velocity of direction ξ^j. Reynolds number is $Re = Cu_m / \nu_l$ (ν_l is the kinematic viscosity of liquid) and it is set to $Re = 1 \times 10^6$. ν_T is the turbulent kinematic viscosity coefficient which is non-dimensionalized.

The Mach number M is a compressibility parameter considered uniform ($M = 0.1$) in the computational domain.

The objective of this calculation includes unsteady phenomena; however, LES is not suitable because it is a 2D calculation. Therefore Reynolds average model is used. The Baldwin-Lomax turbulence model for a single-phase flow is used to calculate ν_T, because there is no turbulence model established for cavitation at the present. This simulation does not account for the interaction between turbulent fluctuations and cavitation, which is our future work.

2.3 Cavitation model

Omitting the second-order derivatives, viscous and surface tension terms in the Rayleigh-Plesset equation derives:

$$\frac{dR}{dt} = \sqrt{2(p_v - p)/3\rho_l} \tag{4}$$

where R is the bubble radius. Eq. (4) gives the increase rate of bubble radius for $p < p_v$. An expansion of square-root gives:

$$\frac{df_l}{dt} = \frac{1-f_l}{\rho_l R}\left(p - p_v\right) \tag{5}$$

This equation simply means that the cavitation region will expand under the condition of $p < p_v$, whereas it will contract in the region of $p > p_v$. It is similar to the model proposed by Chen and Heister [13]: $D\rho/Dt = C\,(p - p_v)$. An empirical constant C in their model seems to be related to the bubble diameter as supposed from Eq. (5). However, R can not be determined because bubbles of varied size are included in the actual cavitating flow. Chen and Heister [13] tested a very wide range of values for C: namely, 500, 5000 and 50000. It may be related to the variation of R. Another problem of Eq. (5) in the actual computation is that the right hand side can not become negative when $f_l = 1$. Considering these problems, Okita and Kajishima [12] proposed:

$$\frac{Df_l}{Dt} = \left\{C_g(1-f_l) + C_l f_l\right\}\left(p - p_v\right) \tag{6}$$

The model constants are C_l = 1 and C_g = 1000 for $p < p_v$ (inception and growth of cavity) whereas C_g = 100 for $p > p_v$ (contraction and disappearance of cavity). These two parameters were determined by comparison of experimental and numerical data of cavitating flow around a rectangular prism. The same values were used by Okita and Kajishima [12], without making any particular adjust for the current calculation.

2.4 Computational method

The time marching procedure is based on the fractional step method. The 2nd order Adams-Bashforth method is used for the convective and viscous terms, and backward Euler method is used for the pressure term and continuity equation (Okita and Kajishima [12], Ohashi and Kajishima [5]). The viscous term is discretized with central differences of 4th order accuracy. A modified upstream difference is applied for the convective term.

3. RESULTS

First, a cavitation number σ = 0.2, 0.3 0.6 is considered for incidence angle α = 3°. And the influence of incidence angle α = 3°, 6°, 9° is considered when cavitation number is fixed to σ = 0.6. Then, the calculation conditions, for example σ = 0.6 and α = 3°, are expressed as Caseσ.6-α3. The other parameters are fixed in common.

A uniform flow is given as initial condition. Then, the flow develops in a single-phase for a designated α. After that, the cavitation condition is set by the value of σ and the unsteady flow field develops enough with the time marching.

The results are summarized in the table 1. It is divided into the parts of odd and even number blades. Small cavities occurred homogeneously for all number of blades near the leading edge on suction side on the Caseσ.6-α3. In this case, cavitation is vibrates and rotates. However, it's possible to consider it quasi-steady and homogeneous because the amplitude of the vibration is very weak. Therefore, this case is excluded in table 1. Except for the N = 4 cases and Caseσ.2-α3, on the three remaining cases, the scale of cavity and the propagation speed varies depending on the flow parameters, but the qualitative behavior is almost similar.

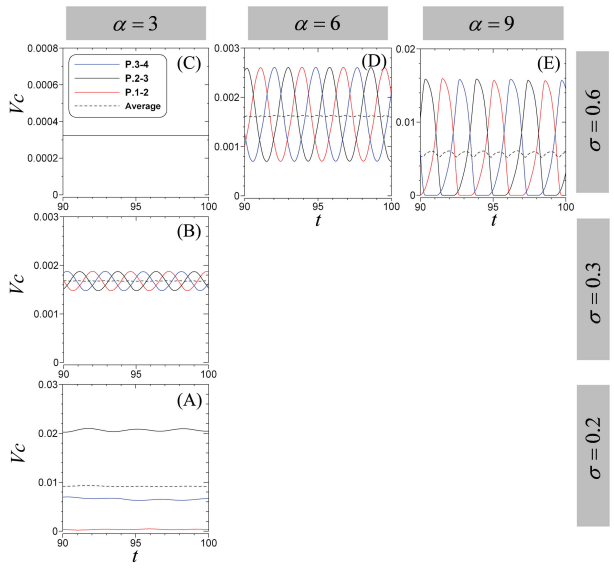

Figure 2: Influence of σ and α on time evolution of cavitation volume in each passage of a 3-blades cascade

3.1 Cascades of 3- and 4-blades

A result for 3-blades cascade is shown in this section. A part of this case was treated in the past research [6].

Fig. 2, show temporal evolution of the cavity volume Vc in each flow passage. A uniform and quasi-steady state cavitation is observed in Caseσ.6-α3 (C), but a weak rotating cavitation is observed in Caseσ.3-α3 (B) which lowered σ. Furthermore, cavitation turns into quasi-steady state in Caseσ.2-α3 (A). For this case, cavitation turns into the super cavitation state, namely when the area of a cavity reaches a trailing edge. On the other hand, rotating cavitation is observed in Caseσ.6-α6 (D), when the incidence angle α is increased and the cavitation number σ is fixed 0.6. Moreover, in Caseσ.6-α9 (E), the cavity volume changes drastically, and the wave pattern is also distorted.

In 3-blades cascade, for all unsteady state, the flow passages that cavitation volume Vc becomes biggest are moving to the rotating direction. Therefore, these are distinguished as forward rotating cavitation. In table 1, this is expressed with '+1' in rotating direction, but '-2' also is wrote in the same column because the 1st flow passage is same the 2nd it to opposite direction in case of 3-blades cascade. The propagation becomes slower for larger Vc. In addition, when rotating cavitation is observed, all of it is partial cavitation.

In Caseσ.3-α3, σ.6-α6 and σ.6-α9, the cavity rotates. There are cavities in all passages, except in Caseσ.6-α9. The black dashed lines in Fig. 2 show the mean of the cavity volume between all flow passages. Except in Caseσ.6-α9, the mean cavity volume in terms of time is almost constant. This anticipates that the whole flow passage system is unstable due to the variation of incidence angle, which becomes larger.

Table 1: Summary of cavity transfer patterns

Number of blades N	Case σ.2 - α3 σ = 0.2, α = 3°	Case σ.3 - α3 σ = 0.3, α = 3°	Case σ.6 - α6 σ = 0.6, α = 6°	Case σ.6 - α9 σ = 0.6, α = 9°
3	Quasi-Steady Asymmetric	Rotating +1, -2 (0.86)	Rotating +1, -2 (0.94)	Rotating +1, -2 (1.15)
5	Rotating (long period) +1, -4 (2.95)	Rotating +3, -2 (0.66)	Rotating +3, -2 (0.78)	Rotating +3, -2 (0.96)
7	Rotating(long period) +4, -3 (3.73)	Rotating +5, -2 (0.52)	Rotating +5, -2 (0.63)	Rotating +5, -2 (0.79)
11	Rotating (long period) +3, -8 (4.27)	Rotating +3, -8 (0.26)	Rotating +3, -8 (0.29)	Rotating +3, -8 (0.36)
4	Rotating(long period) +1, -3 (3.69)	Quasi-Steady Even	Alternate ± 2 (1.53)	Rotating (long period) +3, -1 (3.58)
6	Oscillating Pair	Rotating Pair +4, -2 (0.43)	Rotating Pair +4, -2 (0.47)	Rotating Pair +4, -2 (0.59)
8	Rotating (long period) +3, -5 (4.76)	Rotating +3, -5 (0.38)	Rotating +3, -5 (0.43)	Rotating +3, -5 (0.52)

Numbers, ± m and ( ), indicate the order of appearance and the numbers in parentheses denote *T/N*.

In Fig. 3, the propagation phenomenon is considered based on the vapor volume fraction and the variation of the speed vectors. The solid line near the cavity indicates the difference between the velocity vector and the time-mean flow. It's assumed that a cavity developed on the suction side of the B.2 at some moment (left side of Fig. 3). The blocking effect is caused when the cavity is shrinking, then a new cavity can be generated in B.3, the next passage (middle of Fig. 3), but first, the cavity developing in B.1 reaches its maximum size. Namely, the propagation of the phenomenon is observed in the backward direction (B.2→B.3), but the biggest cavity is observed in the forward direction (B.2→B.1).

As a typical example, see Fig. 4, the cavity volume in each passage between the blades is expressed by a solid line, and the time evolution of the local flow angle at 0.1*C* upstream side from leading edge is expressed by dashed line. The local flow angle increases in opposite direction of rotation when a cavity develops in a certain blade, shown with oval marks. In other words, the phenomenon propagates backward through the dotted line. However, as explained by Fig. 3, the biggest cavity follows the direction of the dash-dot line between the passages. It is corresponding to '+1' in forward direction, but it becomes '-2' in backward direction. In Fig. 4, the 2 dotted lines and the dash-dot line are passing in a certain time. The expression, "two pieces of information are propagating" by Iga et al. [8], is consistent to the result indicated by dotted lines of Fig. 4.

Next, the result of 4-blades cascade is discussed. Fig. 5 is the time change of cavity volume between each passage. Caseσ.3-α3 is quasi-steady and uniform as well as σ.6-α3. On the other hand, unsteady alternate cavitation occurs in Case σ.6-α6. The above-mentioned tendency accords with an observed result by Fortes-Patella [9]. In Caseσ.6-α9 with increased α, and Caseσ.2-α3 with lowered σ, the fluctuation is so long that vapor-phase appears and disappears in some of the passage. Particularly in the latter, the mean of cavity volume at all passages also fluctuates remarkably, and unstableness as a system is suggested.

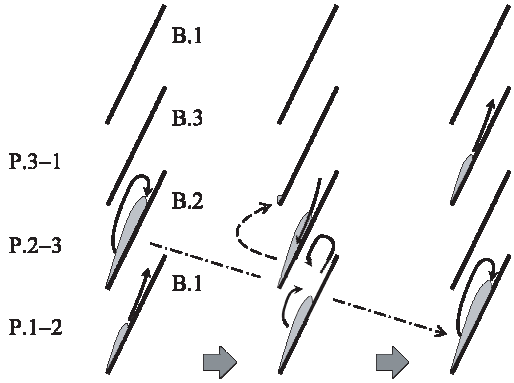

Figure 3: Typical pattern of cavity propagation (solid lines: flow; dashed lines: trigger; dash-dot lines: transfer)

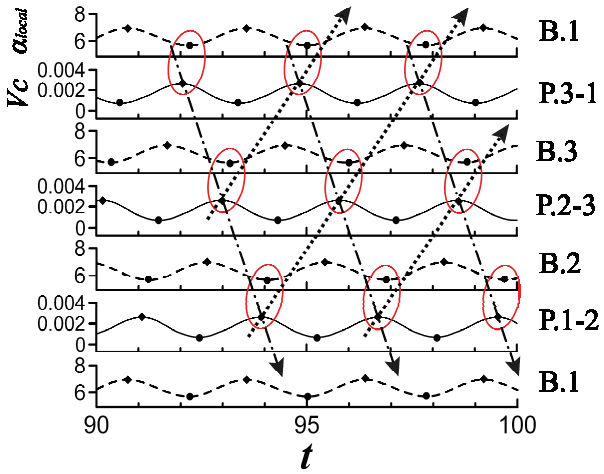

Figure 4: Time evolutions of local flow angle (dashed lines) and cavity volume (solid lines) in each passage of $N = 3$; Case σ.6- α6

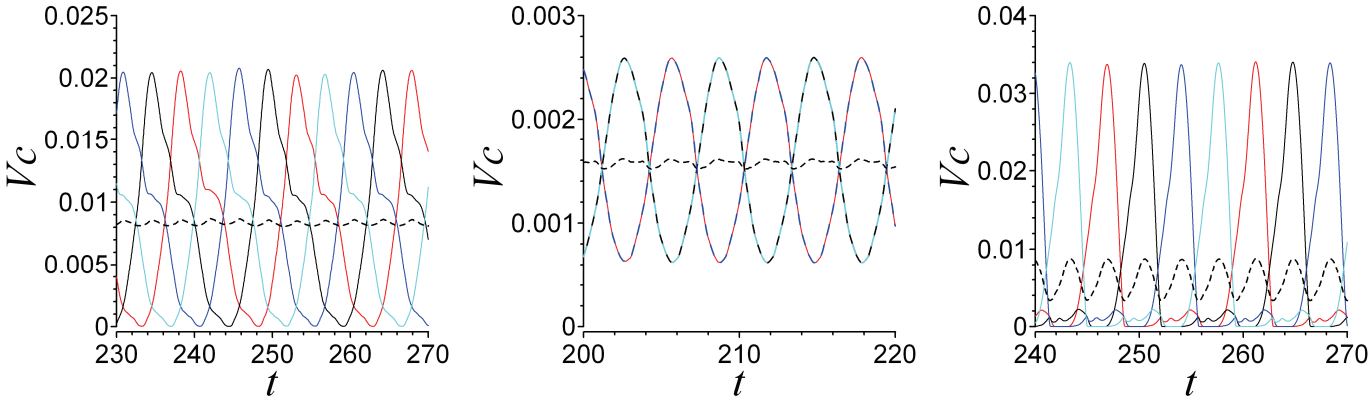

Figure 5: Influence of σ and α on time evolution of cavitation volume in each passage of 4-blades cascade (red lines: P.1-2; black lines: P.2-3; blue lines: P.3-4; sky-blue lines: P.4-1; black dashed lines: average)

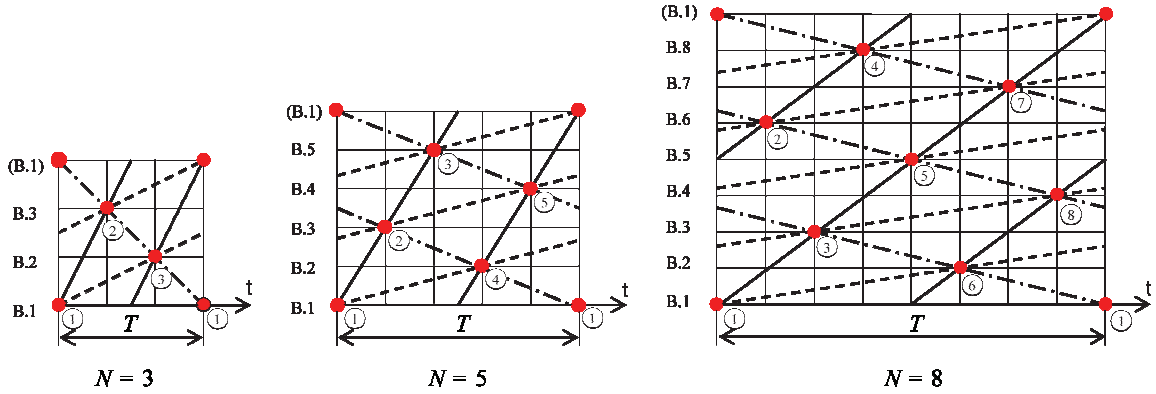

Figure 6: Chart for propagations of maximum cavitation (●): trigger (‘-1’, dashed lines), basic mode (‘-2’, solid lines) and forward rotation (‘+1’, dash-dot lines)

However, alternate cavitation is hard to distinguish whether meaning every 1 (±2) or rotating symmetry site (±180°).

The above-mentioned results were consistent to the previous studies [8] [9] for 3- and 4-blades cascade. However, it is difficult to conclude a universal tendency because the influence of the periodicity was strong in small number blades.

3.2 Cascades of a prime number blades

To reduce the influence of the periodicity and find the generality of unsteady cavitation, the results are compared for larger prime number of blades.

In the table 1, there is a common characteristic about propagation of the rotating cavitation for Caseσ.3-α3, σ.6-α6, σ.6-α9 with N = 3, 5, 7. Namely, relative positions of the propagation of maximum cavity is ‘+1’ (N = 3), ‘+3’ (N = 5), ‘+5’ (N = 7) to the forward, respectively, but it is always `-2' to the backward.

From Table 1, Fig. 3 and Fig. 4, in cases of N = 3, 5, 7, the cavity has an influence on the incidence angle of passage ‘-1’, which is next to the backward side, but, the passage where the cavity clarifies is ‘-2’ relatively. The forward rotating ‘+1’ observed in case of 3-blades is included in this universality.

In table 1, the correlation called ‘-2’ is not seen in case of larger prime numbers such as N = 11. This is because more than one cavitation is rotating at the same time, due to the increased number of blades. The method of discrimination is discussed in Sec. 3.4.

Cavitation fluctuates for a very long period in Caseσ.2-α3 for N = 5, 7, 11. The wave pattern resembles the condition of N = 4 (left side of Fig. 5), but it becomes more complicated with the increase of N. On the other hand, the non-uniform and quasi-steady state (Caseσ.2-α3 (A) of Fig. 2) seems to be limited to a cascade with a small number of blades like N = 3.

3.3 Cascades of an even number blades

The problem if whether alternating cavitation mode exists stably or not is left in case of even number blades. Here the results of 6- and 8-blades are considered.

In case of 6-blades, a strong correlation is observed in the two passages of rotating symmetry, namely, B.1 and B.4, B.2 and B.5, B.3 and B.6. The size of three sets of cavities becomes non-uniform in Caseσ.2-α3, and the cavity becomes big in a particular set of passages facing each blade, but it doesn't rotate. On the other hand, three pairs rotate in Caseσ.3-α3, σ.6-α6 and σ.6-α9. From the viewpoint of rotating cavitation that the correlation is strong as ‘-2’, the tendency is the same for N = 3, 5, 7. On the other hand, as for the pairs of cavity in the rotating symmetry, the influence of N = 4 remains. In case of N = 6, not "the alternation" seen in N = 4, but the rotating pair manifests.

In case of the 8-blades cascade, cavitation is not observed

alternately, but the rotating cavitation becomes dominant. Namely, rotating cavitation is observed in the cascade of even numbers of blades. In cases of N = 4 and 6, they are likely to form a pair. However, the simultaneous appearance of two cavities in the rotating-symmetry position can not be observed in N = 8. Thus the pair mode is thought to be a particular phenomenon observed in small even numbers.

3.4 Generality of rotation cavitation

A general characteristic about Caseσ.3-α3, Caseσ.6-α6 and Caseσ.6-α9 at cases of the N = 3, 5, 7, 8, 11 is summarized in Table 2. The Fig. 6 diagrams of the propagation in cases of N = 3, 5, 8. The blades (marked ●) in which the cavity reaches it maximum size on the suction side are tied, using dashed lines, solid lines and dash-dot lines. The 'trigger' indicated by dashed lines means that the influence is transmitted to a sequence of '-1', the solid line shows the 'basic' mode '-2'. And the 'forward' mode denoted by dash-dot lines shows the forward rotation '+1'. The three kinds of lines like in Fig. 6, tie up the blades in which the biggest cavity occurs. The numbers of lines that go through the diagram is summarized in Table 2. Then, we can establish a law as follows:

(i) $M_{-1} = M_{-2} + M_{+1}$

(ii) After the biggest cavity occurs in blade I, the sequence that the biggest cavity appears in the backward 2nd is corresponding to the M_{-2} -th counting form I blade.

In other words, we can find the number of simultaneously rotating cavitations is M_{-2} .

The number of propagating information in 3-blades cascade is M_{-1}. It is seen in Fig. 6 that the forward rotating '+1' and the basic mode '-2' tie the same blade to the opposite direction in N = 3.

3.5 Period of rotation cavitation

Fig. 7 shows the period of rotating cavitation for various numbers of blades for some conditions. In the three cases of an odd number, T/N decreases for N linearly. Then, the traverse speed of the cavity is not constant in case of partial rotating cavitation. The period T becomes longer for larger N, which means the reduction of the influence of periodicity, and for longer time-scale of each cavitation.

In cases of an even number, when the number of blades increases, the cavitation is shifted from alternate mode to rotate mode. The result for N = 8 gets closer to the characteristic of the odd number blades. Therefore, it could be stated again that pair mode is a characteristic in case of small number of blades based on this analysis of periodicity.

4. CONCLUSION

The numerical simulations of the cavitating flow in 2D cascades, which modeled a cross section of a liquid fuel rocket engine inducer, were carried out. To consider the generality in the rotating cavitation, we treated two series of blade numbers; namely prime numbers and even numbers in addition to the numbers, 3 and 4, in conventional inducers.

Table 2: Summary of cavity transfer patterns

Number of Blades N	Trigger M_{-1}	Basic M_{-2}	Forward M_{+1}
3	2	1	1
5	3	1	2
7	4	1	3
8	5	2	3
11	7	3	4

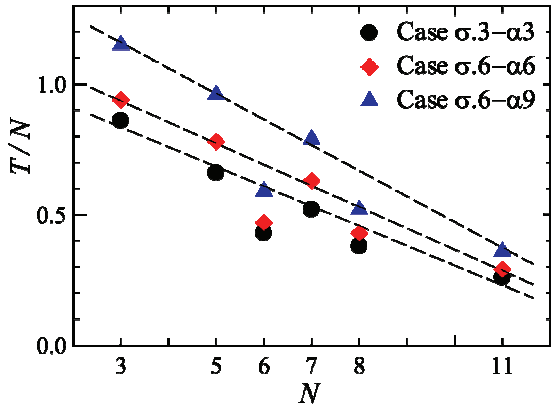

Figure 7: Period of rotating cavitation

At first, the characteristic patterns of steady and unsteady flows observed in 3- and 4-blades cascade could be reproduced. We therefore think our method can be used for qualitative discrimination of unsteady cavitation patterns by a 2D model.

The following generalities were observed in case of rotating patterns for the all blades numbers.

(1) The enhanced cavitation causes next cavitation by increasing the local flow angle at the leading edge of next blade to the backward direction (-1).

(2) But it takes time for growing up, another cavity which has been developing in a different passage grows in advance.

(3) The basic pattern of rotation is every-second-passage of backward direction.

These characteristics include the specialty of small number of blades and the cases of multiple rotating cells in large number of blades. On the other hand, the period of rotation is very long in case of super cavitation and it is transformed to alternate or quasi-steady mode in case of small numbers of blades.

A generality was found about rotating partial cavitation by making a chart that shows the 'trigger' sequence of '-1', the 'basic' mode of '-2' and the 'forward' mode of '+1'. Besides we could find by counting the number that each lines go through at a certain moment. As for the time scale of rotating cavitation, T/N decreased for number of blades N linearly.

ACKNOWLEDGMENTS

This study was supported by the Grant-in-Aid for Scientific Research of the Ministry of Education, Culture, Sports, Science and Technology – Japan. It was also partly supported by a collaborative research project with IHI Co. The authors express their gratitude to the contribution of Dr. Takashi Ohta and Dr. Kohei Okita. And the first author would like to acknowledge the Japanese Ministry of Education, Culture, Sports, Science and Technology, MEXT, for financial support through scholarship program.

NOMENCLATURE

C	Chord length
C_g, C_l	Constants for cavitation model
f_l	Volumetric fraction of liquid phase
h	Pitch of cascade
$J\left(=\left\|\partial x_i / \partial \xi^j\right\|\right)$	Jacobian of coordinate transformation
$M\left(=u_{in}/c\right)$	Mach number (c: speed of sound)
p	Static pressure
p_v	Vapor pressure
p_∞	Static pressure at far upstream
$Re\left(=Cu_{in}/v_l\right)$	Reynolds number
u_i, U^j	Cartesian and contra-variant components of velocity
u_{in}	Inlet velocity
V_c	Volume of cavity
x_i, ξ^j	Cartesian and curvilinear coordinates
α	Incident angle
β	Stagger angle of cascade
v_l	Kinetic velocity of liquid
σ	Cavitation number
ρ_l	Liquid density

REFERENCES

[1] Kamijo, K. and Yoshida, M. 1991, "Experimental study of LE-7 LOX pump inducer," *Trans. JSME*, 57, Series B, 544 (in Japanese), 4023-4028.

[2] Tsujimoto, Y., Kamijo, K. and Yoshida, Y. 1993, "A theoretical analysis of rotating cavitation in inducers," *Trans. ASME, J. of Fluids Engineering*, 115, 135-141.

[3] Tsujimoto, T., Watanabe, S., Kamijo, K. and Yoshida,Y. 1996, "A nonlinear calculation of rotating cavitation in inducers," *Trans. ASME, J. of Fluids Engineering*, 118, 589-594.

[4] Watanabe, S., Sato, K., Tsujimoto, Y., and Kamijo, K. 1999, "Analysis of rotating cavitation in a finit pitch cascade using a closed cavity model and a singularity method," *Trans. ASME*, 121, 834-840.

[5] Ohashi, Y. and Kajishima, T. 2005, "Numerical simulation of rotating cavitation in a 2-D cascade," *Proc. of the 6th KSME-JSME Thermal & Fluids Engineering Conf.*, Jeju, Korea, DG.01(CD).

[6] Ohta, T. and Kajishima, T. 2008, "Transition of different un-steady cavitating flows in 2D cascade with flat blades, "*Proc. 12th Int. Symp. on Transport Phenomena and Dynamics of Rotating Machinery*, Honolulu, Hawaii, USA, ISROMAC12-2008-20197(CD).

[7] Ugajin, H., Kawai, M., Okita, K., Matsumoto, Y., Kajishima, T., Kawasaki, S. and Tomaru, H. 2006, "Numerical simulation of unsteady cavitating flow in a turbo pump inducer," *Proceedings of the 42nd AIAA/ASME/SAE/ASEE Joint Propulsion Conference*, Sacramento, California, USA, AIAA2006-5068(CD).

[8] Iga, Y., Nohmi, M., Goto, A. and Ikohagi, T. 2004, "Numerical analysis of cavitation instabilities arising in the three-blade cascade, " *Trans. ASME, J of Fluids Engineering*, 126, 419-429.

[9] Fortes-Patella, R., Coutier-Delgosha, O., Perrin, J. and Reboud, J. L. 2007, "Numerical model to predict unsteady cavitating flow behavior in inducer blade cascades," *Trans. ASME, J. of Fluids Engineering*, 129, 128-135.

[10] Coutier-Delgosha, O., Fortes-Patella, R., Reboud, J. L., Hakimi, N., and Hirsch, C. 2005, "Numerical simulation of cavitating flow in 2D and 3D inducer geometries," *Int. J. of Numerical Methods in Fluids*, 48, 135-167.

[11] Yamanishi, N., Fukao, S., Qiao, X. G., Kato, C. and Tsujimoto, Y. 2007, "LES simulation of backflow vortex structure at the inlet of an inducer," *Trans. ASME, J. of Fluids Engineering*, 129, 587-594.

[12] Okita. K. and Kajishima, T. 2000, "Numerical investigation of unsteady cavitating flow around a rectangular prism," *Proceedings of the 4th JSME-KSME Thermal Engineering Conference*, Kobe, Japan, 2, 571-576.

[13] Chen, Y.-L. and Heister, S. 1995, "Two-phase modeling of cavitated flows," *Computers & Fluids*, 27, No.7, 799-809.